Long-range transverse Ising model built with dipolar condensates in two-well arrays

2017 New J. Phys. 19 013030

(http://iopscience.iop.org/1367-2630/19/1/013030)

New Journal of Physics
The open access journal at the forefront of physics

Deutsche Physikalische Gesellschaft DPG
IOP Institute of Physics

Published in partnership with: Deutsche Physikalische Gesellschaft and the Institute of Physics

OPEN ACCESS

RECEIVED
17 August 2016

REVISED
8 January 2017

ACCEPTED FOR PUBLICATION
11 January 2017

PUBLISHED
25 January 2017

PAPER

Long-range transverse Ising model built with dipolar condensates in two-well arrays

Yongyao Li[1,2,3], Wei Pang[4], Jun Xu[5,6], Chaohong Lee[6], Boris A Malomed[3] and Luis Santos[7]

[1] School of Physics and Optoelectronic Engineering, Foshan University, Foshan 528000, People's Republic of China
[2] Department of Applied Physics, South China Agricultural University, Guangzhou 510642, People's Republic of China
[3] Department of Physical Electronics, School of Electrical Engineering, Faculty of Engineering, Tel Aviv University, Tel Aviv 69978, Israel
[4] Department of Experiment Teaching, Guangdong University of Technology, Guangzhou 510006, People's Republic of China
[5] Center of Experimental Teaching for Common Basic Courses, South China Agriculture University, Guangzhou 510642, People's Republic of China
[6] TianQin Research Center & School of Physics and Astronomy, Sun Yat-Sen University (Zhuhai Campus), Zhuhai 519082, People's Republic of China
[7] Institut für Theoretische Physik, Leibniz Universität Hannover, Appelstr. 2, D-30167 Hannover, Germany

E-mail: malomed@post.tau.ac.il

Keywords: dipole–dipole interactions, long-range Ising model, Kibble–Zurek scenario, Anderson localization

Abstract

Dipolar Bose–Einstein condensates in an array of double-well potentials realize an effective transverse Ising model with peculiar inter-layer interactions, that may result under proper conditions in an anomalous first-order ferromagnetic–antiferromagnetic phase transition, and non-trivial phases due to frustration. The considered setup allows as well for the study of Kibble–Zurek defect formation, whose kink statistics follows that expected from the universality class of the mean-field one-dimensional transverse Ising model. Furthermore, random occupation of each layer of the stack leads to random effective Ising interactions and local transverse fields, that may lead to the Anderson-like localization of imbalance perturbations.

1. Introduction

A new generation of experiments with ultra-cold magnetic atoms [1–4], polar molecules [5–8], and Rydberg-dressed atoms [9] are starting to reveal novel fascinating physics of dipolar gases. Whereas in non-dipolar Bose gases inter-particle interactions are short-range and isotropic, dipolar gases present significant or even dominant dipole–dipole interactions (DDI), which are long-range and anisotropic. As a result, the physics of dipolar gases strongly differs from that of their non-dipolar counterparts [10, 11], featuring effects such as geometry-dependent stability [12], roton-like excitations [13, 14] and roton-dominated immiscibility [15, 16], strongly anisotropic vortices [17–19] and solitons [20, 21], ferrofluidity [22, 23] and anisotropic superfluidity [24], striped patterns [25], specific mesoscopic configurations trapped in triple potential wells [26], double- and triple-periodic ground states in lattices populated by dipolar atoms [27], and the recent discovery of robust quantum droplets [28, 29].

Dipolar gases in optical lattices are also remarkably different from their non-dipolar counterparts [10, 11]. Whereas in the absence of DDI, interparticle interactions in deep lattices reduce to on-site nonlinearity, the DDI result in inter-site interactions. The latter is true even for very strong lattices, in which inter-site tunneling vanishes. As a result, dipolar lattice gases allow for the transport of excitations in the absence of mass transfer. Recently, spin-like transport was studied in gases of magnetic atoms [4] and polar molecules [6], where the spin was encoded, respectively, in the electronic spin and in the rotational degree of freedom. The dipole-induced spin exchange and Ising interactions result in an effective XXZ Hamiltonian [30, 31]. It has been recently shown that in an imperfectly filled lattice the dipole-induced spin exchange may result in a peculiar disorder scenario [32].

In this paper, we discuss a set-up that permits for coding spin-like systems into a spatial degree of freedom of a dipolar Bose–Einstein condensate (BEC). The condensate is prepared in a stack of layers of two-well potentials

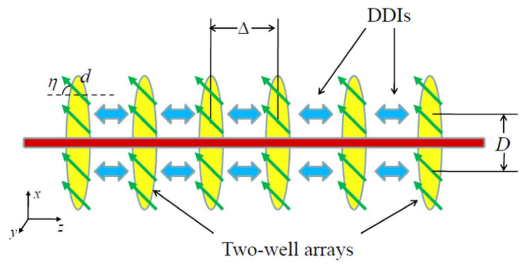

Figure 1. Sketch of the setup considered: a stack of two-well arrays of dipolar condensates formed an effective one-dimensional transverse Ising model.

that emulate an effective spin-1/2 system (see figure 1). This set-up realizes a transverse Ising model with a peculiar form of long-range interactions that results in an unconventional first-order ferromagnetic–antiferromagnetic transition, as well as in phases with anomalous periodicities due to magnetic frustration. Since the parameters may be easily changed in real-time the model allows as well for quenching through second-order phase transitions, as we illustrate for the particular case of a transition from an effective paramagnet into a ferromagnet. We show that the associated defect formation follows the Kibble–Zurek (KZ) [33–35] scaling expected from the universality class of the mean-field one-dimensional transverse Ising model. Furthermore, we show that random layer filling results in an effective disorder in both the Ising-like interactions and the local transverse field, allowing for the observation of Anderson-like localization of imbalance perturbations.

The paper is organized as follows. In section 2 we introduce the set-up and derive the effective long-range transverse Ising model. Section 3 discusses the corresponding ground-state phases, whereas section 4 comments on the formation of KZ defects. Section 5 discusses the effective disorder resulting from random layer filling and the associated Anderson-localization in the imbalance transport. Finally section 6 summarizes our conclusions.

2. The model

We consider in the following a stack of axisymmetric quasi-one-dimensional dipolar BECs ('wires'), separated along the z direction by a distance Δ, with their axes oriented along x, as shown in figure 1. This configuration may be readily created by loading the BEC into just one plane of a 2D optical lattice created in the yz plane. The lattice is assumed deep enough, to suppress both on-site dynamics along the y and z directions and tunneling between adjacent condensates. An additional double-well potential $U(x)$, with inter-well spacing D, is placed along the x axis, while the atomic dipole moments are parallel to the xz plane, forming angle η with the z axis. The system is described by a set of coupled one-dimensional Gross–Pitaevskii (GP) equations:

$$\mathrm{i}\hbar\frac{\partial}{\partial t}\psi_n(x,\,t) = \left[-\frac{\hbar^2}{2m}\frac{\partial^2}{\partial x^2} + U(x) + \mathcal{V}_n(x)\right]\psi_n(x,\,t), \tag{1}$$

with m the particle mass, $\psi_n(x,\,t)$ the axial wave function at site n, and

$$\mathcal{V}_n(x) \equiv \int_{-\infty}^{+\infty} \mathrm{d}x'\left[\sum_{n'} V_{n'-n}(x-x') + g_{1D}\delta(x-x')\delta_{n'n}\right]|\psi_{n'}(x',\,t)|^2. \tag{2}$$

The contact interactions are characterized by $g_{1D} = \frac{2\hbar^2 a}{ml^2}$, with a the scattering length, and l the effective oscillator length associated to the on-site confinement in the yz plane. $V_{n'-n}(x)$ is the DDI between dipoles placed $n'-n$ sites apart and separated by an axial distance x. The kernel $V_{n'-n}(x)$ is the Fourier transform of

$$\tilde{V}_{n'-n}(k_x) = \int\frac{\mathrm{d}k_y}{2\pi}\int\frac{\mathrm{d}k_z}{2\pi}\tilde{V}_{\mathrm{dd}}(\vec{k})\,\mathrm{e}^{-\mathrm{i}k_z(n'-n)\Delta}\mathrm{e}^{-(k_y^2+k_z^2)l^2/2}, \tag{3}$$

with $\tilde{V}_{\mathrm{dd}}(\vec{k}) = \frac{4\pi}{3}d^2[3|\vec{k}|^{-2}(k_z\cos\eta + k_x\sin\eta)^2 - 1]$ and d the dipole moment.

For a sufficiently tight $U(x)$ potential, we may employ a simplified two-mode scenario in which only the two lowest eigenstates of $U(x)$ participate in the dynamics, $(R(x) \pm L(x))/\sqrt{2}$, where $R(x)$ ($L(x)$) denote the wave functions at the right (left) well. We may then express $\psi_n(x,\,t) = a_n(t)L(x) + b_n(t)R(x)$. The two wells are coherently coupled by a hopping rate J[8]. Under these conditions, the coupled GP equation (1) reduce to

[8] The realization of a coherent Josephson-like coupling between the sites demands a tight-enough axial potential such that quantum or thermal phase fluctuations along the quasi-one-dimensional wires, and hence between the sites, can be neglected. Moreover, due to the assumed weakly interacting nature of the system, quantum fluctuations of inter-site Bogoliubov excitations are not expected to affect the qualitative nature of the phases or phase transitions discussed in this paper, but rather lead to slight displacements of the phase boundaries.

$$\mathrm{i}\dot{a}_n(t) = -Jb_n(t) + \tilde{\mu}_n(t)a_n(t), \tag{4}$$

$$\mathrm{i}\dot{b}_n(t) = -Ja_n(t) + \tilde{\mu}'_n(t)b_n(t), \tag{5}$$

where

$$\tilde{\mu}_n(t) \equiv \sum_{n'}[(\tilde{F}_0(n'-n) + U_0\delta_{n'n})\,|a_{n'}(t)|^2 + \tilde{F}_0(n'-n)\,|b_{n'}(t)|^2]N_{n'}, \tag{6}$$

$\tilde{\mu}'$ is defined with $a_n \rightleftarrows b_n$, $U_0 \equiv g_{1D}\int_{-\infty}^{+\infty}\mathrm{d}x|R(x)|^4$, $\tilde{F}_0(n'-n) \equiv \int_{-\infty}^{+\infty}\mathrm{d}x\int_{-\infty}^{+\infty}\mathrm{d}x' V_{n'-n}(x-x')$ $|R(x)|^2|R(x')|^2$ denotes the interaction between right wells at two sites placed $n\Delta$ apart (or equivalently between left wells), $\tilde{F}_1(n'-n) \equiv \int_{-\infty}^{+\infty}\mathrm{d}x\int_{-\infty}^{+\infty}\mathrm{d}x' V_{n'-n}(x-x')|A(x)|^2|B(x')|^2$ is the interaction between left and right wells, and N_n denotes the number of particles in the nth wire. Since we assume a vanishing inter-site hopping, N_n is conserved, and $|a_n|^2 + |b_n|^2 = 1$. In the following, we assume that the scattering length is tuned by means of Feshbach resonances, so that $U_0 = \tilde{F}_1(0) - \tilde{F}_0(0)$. In this way, the on-site (dipolar plus contact) interactions cancel, allowing us to concentrate on the non-trivial dynamics arising from the inter-layer DDI. Finally, although the exact form of $\tilde{F}_0(n'-n)$ and $\tilde{F}_1(n'-n)$ may be evaluated exactly, we may further simplify the model by considering a point-like approximation that yields

$$\frac{F_0(n'-n)}{d^2/\Delta^3} = \frac{1-3\cos^2\eta}{(n'-n)^3},$$

$$\frac{F_1(n'-n)}{d^2/\Delta^3} = \frac{1}{[(n'-n)^2+(D/\Delta)^2]^{3/2}} - \frac{3[(n'-n)\cos\eta + (D/\Delta)\sin\eta]^2}{[(n'-n)^2+(D/\Delta)^2]^{5/2}}. \tag{7}$$

The exact evaluation of F_0 and F_1 may modify these values, especially for nearest-neighboring wires for which the finite wave packet spreading may be significant compared to the inter-site spacing, but our results would remain qualitatively unaffected.

3. Ground-state phases

Interestingly, the system under consideration is equivalent to a spin-1/2 transverse Ising model with peculiar long-range Ising interactions given by the Hamiltonian

$$H = -J\sum_n N_n S_n^x + \frac{1}{2}\sum_{n,n'} N_n N_{n'} V_S(n-n')S_n^z S_{n'}^z, \tag{8}$$

where $-J$ plays the role of an effective transversal magnetic field, $V_S(n'-n) \equiv [F_0(n'-n) - F_1(n'-n)]/2$ characterizes an effective Ising-like coupling, and we have introduced the effective spin components $S_n^x = a_n^* b_n$ + c.c and $S_n^z = |b_n|^2 - |a_n|^2$.

At this point, we assume that all layers are equally populated, $N_n \equiv N$ (we relax this condition in section 5). We fix the hopping rate as the energy unit, i.e. $J = 1$, and also set $D = 1$. The strength of the DDI is characterized by the parameter $P = Nd^2/J\Delta^3$, which plays a key role in the discussion below. For the particular case of dysprosium atoms with an inter-wire separation of $\Delta = 1\ \mu$m, $d^2/\Delta^3 \sim 1$ Hz, and hence for $N = 10^3$–10^4 atoms, $Nd^2/\Delta^3 = 1$–10 kHz. The corresponding value of P depends on J, which is controlled by the barrier of the two-well potential $U(x)$. For typical values $J \sim 100$ Hz, $P \sim 100$ may be hence readily reached.

The ground-state phase diagram of the system (see footnote 8), presented in figure 2, is obtained numerically from the imaginary-time evolution of equations (4) and (5). If η is such that $V_S(n'-n) < 0$, the Ising interaction is ferromagnetic. For $P/J = 0$ the ground-state of the system is given by a spin oriented along the transversal magnetic field, i.e., along x-axis, and hence a solution with zero imbalance $S_n^z = 0$ is favored. This ground state corresponds to the paramagnetic (Pa) phase. For a sufficiently large $P > P_{\mathrm{cr}}$ ($P_{\mathrm{cr}} \simeq 0.45J$ for $\eta = 0$), the system experiences a second-order phase transition into a ferromagnetic (F) phase, characterized by a full imbalance, either to the R or to the L well. At $\eta_{\mathrm{cr}} \approx 0.33\pi$, $V_S(1) = 0$ and hence the nearest-neighbor (NN) interaction changes the sign. As a result for $\eta > \eta_{\mathrm{cr}}$ at a sufficiently large P/J the system enters an Ising anti-ferromagnetic (AF) phase, characterized by a staggered imbalance between neighboring wires. The situation is obviously reversed for $P < 0$ (which may be achieved by means of a rotating magnetic field [36]), and the Pa–AF transition occurs for $\eta < \eta_{\mathrm{cr}}$ and Pa–F for $\eta > \eta_{\mathrm{cr}}$.

The situation is particularly noteworthy in the vicinity of η_{cr}. Whereas for $P < P_{\mathrm{cr}}(\eta_{\mathrm{cr}}) \approx 147$, the F and AF phases remain separated by a Pa phase, for $P > P_{\mathrm{cr}}(\eta_{\mathrm{cr}})$ there is a first-order F–AF phase transition, see

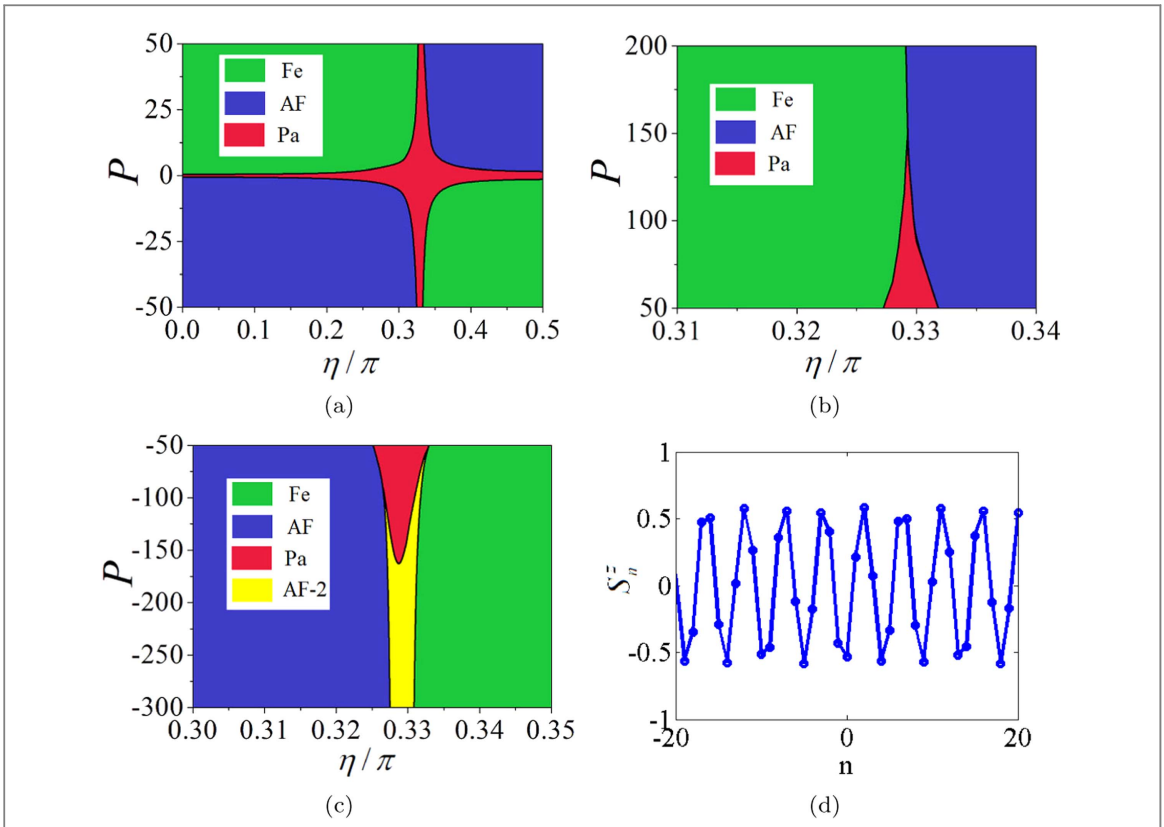

Figure 2. (a) Ground-state phase diagram as a function of the DDI strength $P = Nd^2/J\Delta^3$ and the angle η. (b) Vicinity of η_{cr} for $P > 0$, showing the first-order F–AF transition. (c) Vicinity of η_{cr} for $P < 0$, showing the appearance of the AF-2 phase. (d) AF-2 phase for $\eta = \eta_{cr}$ and $P = -180$; note the formation of an AF order with a periodicity of approximately five wires.

figure 2(b). The reason for this change is that, when $|V_S(1)| < |V_S(2)|$ at $\eta = \eta_{cr}$, $V_S(2)$ remains negative, i.e., $V_S(2)$ favors ferromagnetism between next-nearest-neighbors (NNN). This is both compatible with Néel ordering and with a fully ferromagnetic state. The only difference between these two choices is the orientation between NN, which steeply changes when $V_S(1)$ changes its sign. This is remarkably different from the usual situation in NN Ising models, with $V_S(n > 1) = 0$, in which the change of the sign of $V_S(1)$ implies vanishing interactions, and hence the Pa phase always separates the F and AF phases. It is also different from the standard version of the long-range transverse Ising model induced by dipolar interactions, i.e., $V_S(n' - n) = V_0/(n' - n)^3$. In that case, the change of the NN coupling at $V_0 = 0$ from F to AF also implies vanishing of all interactions, and hence the existence of an intermediate Pa phase. Here, when $P > P_{cr}(\eta_{cr})$, $V_S(1)$ is negligible, and $V_S(2)$ dominates. Such a dominating ferromagnetic NNN coupling allows for a direct first-order transition between F and AF as a function of η.

A similar competition at $P < 0$ results in magnetic frustration. In the vicinity of η_{cr}, when $|V_S(1)| < |V_S(2)|$, one has $V_S(2) > 0$. Under these conditions, the system experiences frustration, as AF NNN interactions are now incompatible with the small F or AF NN coupling. As a result, in the vicinity of η_{cr}, a new phase (AF-2) develops, see figure 2(c), with an approximate five-site-periodic modulation of the imbalance, see figure 2(d).

4. KZ scenario

As shown in section 3 varying P and/or η permits accessing various second-order phase transitions. We note that both parameters may be modified in real time. In particular P may be readily modified by altering the barrier between the two wells, since the latter controls the value of J. This provides the possibility of quenching in real time through the second-order phase transitions of figure 2. Quenching at a finite speed is expected to induce defects due to the KZ mechanism [33–35] .

We illustrate this possibility with the particular case of the Pa–F transition. Increasing P for $\eta = 0$ eventually quenches from the fully balanced Pa phase into the F one. As a result, the system develops F domains, i.e. regions with total imbalance biased to the R or L sites, separated by a domain wall (kink). In our simulations of equations (4) and (5), we consider a balanced input with a slight random imbalance and relative phase

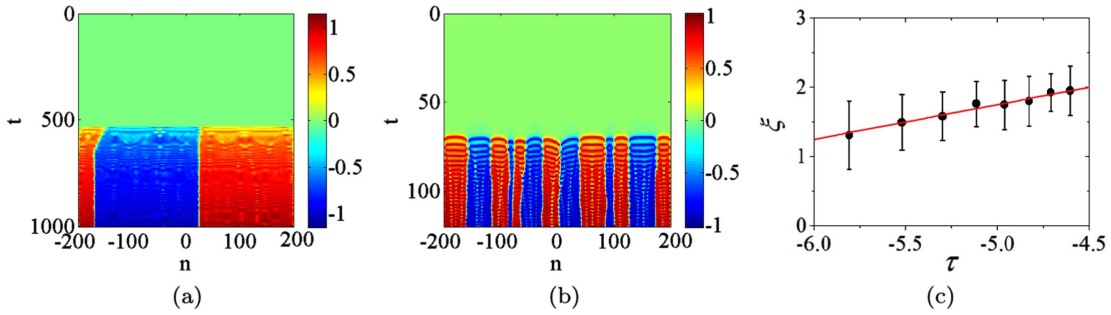

Figure 3. Pattern formation in the imbalance distribution as a function of time for $\eta = 0$ and a linear ramp $P(t) = \gamma t$ with a ramp speed $\gamma = 10^{-3}$ (a) and 10^{-2} (b); (c) $\xi = \ln N_D$, where N_D is the number of domains, as a function of $\tau \equiv \ln \gamma$, the results being best fitted by $\xi = 4.25 + 0.5\tau$, which implies that $N_D \propto \gamma^{1/2}$, as expected from the KZ scaling.

perturbation: $a_n = (0.5 - \varepsilon\ \rho_1)^{1/2} \exp(\mathrm{i}\varepsilon\ \rho_2)$ and $b_n = (0.5 + \varepsilon\ \rho_1)^{1/2} \exp(-\mathrm{i}\varepsilon\ \rho_2)$, where $-1 < \rho_{1,2} < 1$ are two sets of random numbers, and $\varepsilon \ll 1$ (10^{-6} in our calculations) is the strength of the randomness. This small randomness mimics slight imperfections that seed the domain-wall formation. We then impose a linear ramp, $P(t) = \gamma t$, with different ramp speeds γ. Typical numerical results for two values of γ are displayed in figures 3(a) and (b). As expected, the number of kinks increases with the ramp speed γ when crossing the transition. From a large number of random realizations (up to 50 different sets of $\rho_{1,2}$), we extract, for each value of γ, statistics of the number of the domain walls, N_D. Figure 3(c) depicts $\ln(N_D)$ as a function of $\ln(\gamma)$, showing that $N_D \sim \gamma^{1/2}$. The later follows the known KZ scaling, $N_D \sim \gamma^{\nu/(\nu z+1)}$, where $\nu = 1$ and $z = 1$ are the critical static and dynamical exponents for the mean-field one-dimensional transverse Ising model [35].

5. Imbalance transport in the presence of random fillings

The coupling between layers in equation (8) crucially depends on the number of particles in each layer. This opens interesting possibilities for the study of excitation transport—in particular, localization due to random interactions, rather than due to random hopping (we recall that mass transport between wires is suppressed). We consider a randomized distribution of the number of particles in each wire, $N_n/N = 1 + \varepsilon R_n$, where $-1 < R_n < 1$ are random numbers, and $\varepsilon \in [0,\ 1]$ determines the strength of the randomness. Such random distributions may be created by abruptly growing the lattice on top of a trapped BEC. Note that the random population in each wire translates into a random inter-wire interaction in equation (8), which may significantly affect the transport of imbalanced excitations.

We here consider an initially localized imbalance excitation on top of an otherwise perfectly balanced system, i.e., $a_n = b_n = 1/\sqrt{2}$ for all n, except for $a_0 = 1$ and $b_0 = 0$ at $n = 0$. In the following, we focus on $\eta = 0$ and fix $P = 0.1 < P_{\mathrm{cr}}$ (note that, for $P > P_{\mathrm{cr}}$, the balanced background would be unstable). To study more accurately the effect of the disorder on the imbalance transport, we analyze a large number, $K = 500$, of random realizations. Figure 4 shows the average spatial profile of the imbalanced perturbation, $\overline{S_n^z}(t) = K^{-1}\sum_{s=1}^{K} |S_n^{z(s)}(t)|$, where $S^{z(s)}$ is the imbalance distribution of the sth realization. When $\varepsilon = 0$, the system is homogeneous, and the initial perturbation propagates ballistically, as seen in figure 4(a). In contrast, at $\varepsilon \neq 0$, the expansion from the input defect at $t = 0$ is no longer ballistic, the initial imbalanced perturbation localizing around the center, as shown in figures 4(b) and (c). The respective imbalance profile at $t = 200$ is displayed in figure 4(d). At sufficiently large ε, the imbalanced perturbation remains exponentially localized, resembling Anderson localization. As shown in figure 5, localization is best quantified by monitoring the mean size of the imbalanced perturbation, $\overline{L}(t) = K^{-1}\sum_{s=1}^{K} L^{(s)}(t)$, with

$$L^{(s)}(t) = \sqrt{\frac{\sum_n n^2 |S_n^{z(s)}|}{\sum_n |S_n^{z(s)}|}} \tag{9}$$

being the width of the imbalance distribution of the sth realization. The localization length reduces to few wires when $\varepsilon > 0.5$.

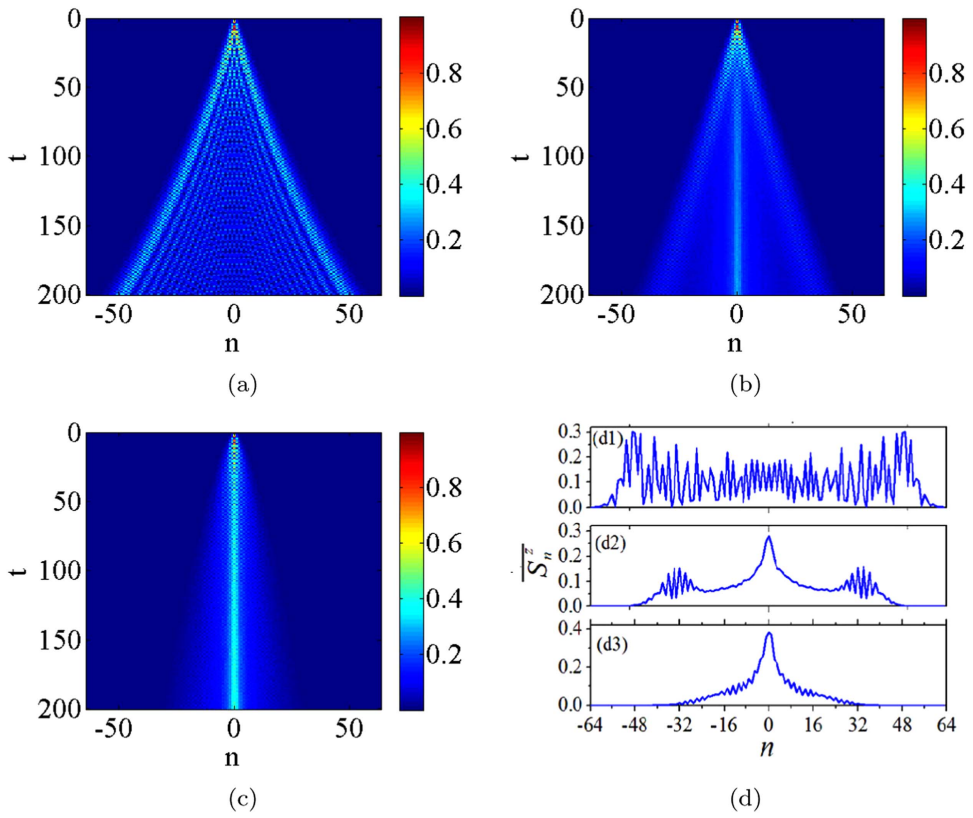

Figure 4. Averaged imbalance distribution $\overline{S_j^z}(t)$ for an initial imbalance perturbation localized at the site $n = 0$, with $\eta = 0, P = 0.1$, and a disorder strength (see text) $\varepsilon = 0$ (a), 0.4 (b), and 0.8 (c). Figure (d) shows from top to bottom $\overline{S_n^z}(t = 200)$ for $\varepsilon = 0, 0.4$, and 0.8.

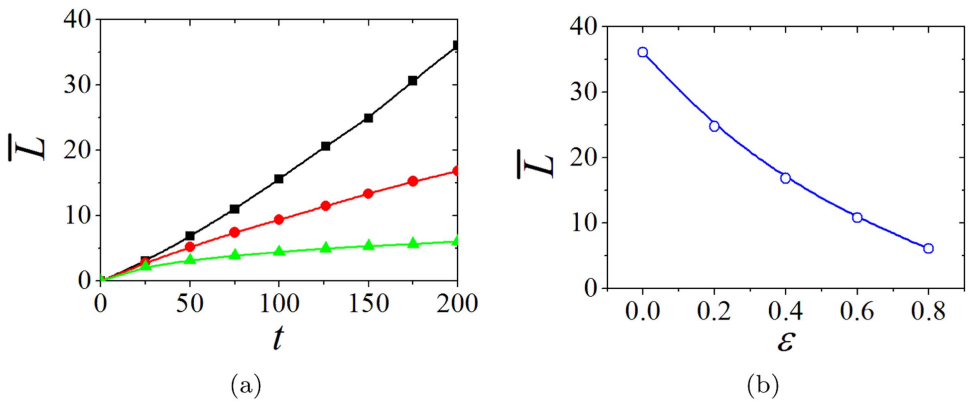

Figure 5. For the same case of figure 4: (a) width $\overline{L}(t)$ for $\varepsilon = 0$ (black squares), 0.4 (red circles) and 0.8 (green triangles); (b) $\overline{L}(t = 200)$ as a function of the disorder strength ε.

6. Conclusions

In summary, dipolar BECs in an array of double-well potentials offer a simple setup which makes it possible to employ the motional degrees of freedom for realizing an effective mean-field transverse Ising model with peculiar inter-layer interactions. The system gives rise to an anomalous first-order ferromagnetic–antiferromagnetic transition, as well as to non-trivial phases induced by frustration. As the parameters can be easily modified in real time, the introduced setup allows as well the study of KZ defect-formation. Furthermore, random occupation in each layer results in random Ising interactions and random effective local transverse fields, which may be employed to controllably study Anderson-like localization of imbalanced perturbations.

Acknowledgments

This work was supported by National Natural Science Foundation of China through grants No. 11575063, No. 11374375 and No. 11574405, by the German-Israel Foundation through grant No. I-1024-2.7/2009, and by the Tel Aviv University in the framework of the 'matching' scheme for a postdoctoral fellowship of YL. The work of BAM, is supported, in part, by the joint program in physics between the National Science Foundation (US) and Binational Science Foundation (US-Israel), through Grant No.2015616. LS thanks the support of the DFG (RTG 1729, FOR 2247).

References

[1] Griesmaier A, Werner J, Hensler S, Stuhler J and Pfau T 2005 *Phys. Rev. Lett.* **94** 160401
[2] Lu M, Burdick N Q, Youn S H and Lev B L 2011 *Phys. Rev. Lett.* **107** 190401
[3] Aikawa K, Frisch A, Mark M, Baier S, Rietzler A, Grimm R and Ferlaino F 2012 *Phys. Rev. Lett.* **108** 210401
[4] de Paz A, Sharma A, Chotia A, Maréchal E, Huckans J H, Pedri P, Santos L, Gorceix O, Vernac L and Laburthe-Tolra B 2013 *Phys. Rev. Lett.* **111** 185305
[5] Ni K K, Ospelkaus S, de Miranda M H G, Péer A, Neyenhuis B, Zirbel J J, Kotochigova S, Julienne P S, Jin D S and Ye Y 2008 *Science* **322** 231
[6] Yan B, Moses S A, Gadway B, Covey J P, Hazzard K R A, Rey A M, Jin D S and Ye J 2013 *Nature* **501** 521
[7] Takekoshi T, Reichsöllner L, Schindewolf A, Hutson J M, Sueur C R L, Dulieu O, Ferlaino F, Grimm R and Nägerl H 2014 *Phys. Rev. Lett.* **113** 205301
[8] Park J W, Will S A and Zwierlein M W 2015 *Phys. Rev. Lett.* **114** 205302
[9] Balewski J B, Krupp A T, Gaj A, Hofferberth S, L öw R and Pfau T 2014 *New J. Phys.* **16** 063012
[10] Lahaye T, Menotti C, Santos L, Lewenstein M and Pfau T 2009 *Rep. Prog. Phys.* **72** 126401
[11] Baranov M A, Dalmonte M, Pupillo G and Zoller P 2012 *Chem. Rev.* **112** 5012
[12] Koch T, Lahaye T, Metz J, Fröhlich B, Griesmaier A and Pfau T 2008 *Nat. Phys.* **4** 218
[13] Santos L, Shlyapnikov G V and Lewenstein M 2003 *Phys. Rev. Lett.* **90** 250403
[14] Wilson R M, Ronen S, Bohn J L and Pu H 2008 *Phys. Rev. Lett.* **100** 245302
[15] Wilson R M, Ticknor C, Bohn J L and Timmermans E 2012 *Phys. Rev.* A **86** 033606
[16] Young-S L E and Adhikari S K 2012 *Phys. Rev.* A **86** 063611
[17] Kawaguchi Y, Saito H and Ueda M 2006 *Phys. Rev. Lett.* **96** 080405
[18] Yi S and Pu H 2006 *Phys. Rev.* A **73** 061602
[19] Abad M, Guilleumas M, Mayol R, Pi M and Jezek D M 2009 *Phys. Rev.* A **79** 063622
[20] Tikhonenkov I, Malomed B A and Vardi A 2008 *Phys. Rev. Lett.* **100** 090406
[21] Nath R, Pedri P and Santos L 2009 *Phys. Rev. Lett.* **102** 050401
[22] Lahaye T, Koch T, Fröhlich B, Fattori M, Metz J, Griesmaier A, Giovanazzi S and Pfau T 2007 *Nature* **448** 672
[23] Saito H, Kawaguchi Y and Ueda M 2009 *Phys. Rev. Lett.* **102** 230403
[24] Ticknor C, Wilson R M and Bohn J L 2011 *Phys. Rev. Lett.* **106** 065301
Wood A A M, Kellar B H J and Martin A M 2016 *Phys. Rev. Lett.* **116** 250403
[25] Macia A, Hufnag D, Mazzanti F, Boronat J and Zillich R E 2012 *Phys. Rev. Lett.* **109** 235307
[26] Lahaye T, Pfau T and Santos L 2010 *Phys. Rev. Lett.* **104** 170404
[27] Maluckov A, Gligorić G, Hadžievski L, Malomed B A and Pfau T 2012 *Phys. Rev. Lett.* **108** 140402
[28] Kadau H, Schmitt M, Wenzel M, Wink C, Maier T, Ferrier-Barbut I and Pfau T 2016 *Nature* **530** 194
[29] Ferrier-Barbut I, Kadau H, Schmitt M, Wenzel M and Pfau T 2016 *Phys. Rev. Lett.* **116** 215301
[30] Micheli A, Brennen G K and Zoller P 2006 *Nat. Phys.* **2** 341
[31] Gorshkov A V, Manmana S R, Chen G, Ye J, Demler E, Lukin M D and Rey A M 2001 *Phys. Rev. Lett.* **107** 115301
[32] Deng X, Altshuler B L, Shlyapnikov G V and Santos L 2016 *Phys. Rev. Lett.* **117** 020401
[33] Kibble T W B 1980 *Phys. Rep.* **67** 183
[34] Zurek W H 1996 *Phys. Rep.* **276** 177
[35] Dziarmaga J 2010 *Adv. Phys.* **59** 1063
[36] Giovanazzi S, Görlitz A and Pfau T 2002 *Phys. Rev. Lett.* **89** 130401